

## Pulsating red giant and supergiant stars in the Local Group dwarf galaxy Andromeda I

Elham Saremi<sup>1</sup> · Abbas Abedi<sup>1</sup> · Atefeh Javadi<sup>2</sup> · Jacco van Loon<sup>3</sup> · Habib Khosroshahi<sup>2</sup>

<sup>1</sup> Department of Physics, Faculty of Science, University of Birjand, Birjand, P.O.Box 97175-615, Iran; email: saremi@birjand.ac.ir

<sup>2</sup> School of Astronomy, Institute for Research in Fundamental Sciences (IPM), Tehran, P.O.Box 19395-5531, Iran;

<sup>3</sup> Lennard-Jones Laboratories, Keele University, ST5 5BG, UK

**Abstract.** We have conducted an optical long-term monitoring survey of the majority of dwarf galaxies in the Local Group, with the Isaac Newton Telescope (INT), to identify the long period variable (LPV) stars. LPV stars vary on timescales of months to years, and reach the largest amplitudes of their brightness variations at optical wavelengths, due to the changing temperature. They trace stellar populations as young as  $\sim 30$  Myr to as old as  $\sim 10$  Gyr whose identification is one of the best ways to reconstruct the star formation history.

The system of galactic satellites of the large Andromeda spiral galaxy (M 31) forms one of the key targets of our monitoring survey. In this first paper in the series, we present the first results from the survey in the form of a census of LPV stars in Andromeda I (And I) dwarf galaxy.

Photometry was obtained for 10585 stars in a 0.07 square degree field, of which 116 stars were found to be variable, most of which are Asymptotic Giant Branch (AGB) stars. Our data were matched to mid-infrared photometry from the *Spitzer* Space Telescope, and to optical catalogues of variable stars from the *Hubble* Space Telescope.

*Keywords:* stars: evolution, stars: red giants, supergiants, stars: mass-loss, stars: oscillations, galaxies: individual: Andromeda I, galaxies: stellar content

## 1 Introduction

Dwarf galaxies are the most common type of galaxies in the Universe, and the building blocks of more massive galaxies in hierarchical formation scenarios. The great variety in terms of stellar mass, luminosity, gas content, metallicity and surface brightness reflect the complex dynamical and astrophysical processes that drive galaxy evolution. Also, they represent the smallest scales on which astronomers are able to detect dark matter [1, 2, 3, 4, 5]. Therefore, their study is crucial for improving the cosmological models and our understanding of galaxy evolution. Naturally, our home, the Local Group (LG), is the best place to study dwarfs since their individual stars can be resolved and evolutionary histories can be derived in great detail.

The LG comprises dwarf galaxies of all diversity: dwarf spheroidals (dSphs), dwarf irregulars (dIrrs), and transition (dTrans) galaxies. dSphs are found in denser environments and have lower luminosities than dIrrs. They show no evidence of recent star formation (within the last 200 Myr). dTrans are located in similar environments occupied by dIrr galaxies; however, their luminosity and the star formation history are more comparable to dSphs [6, 7, 8, 9, 10, 11].

We have conducted an optical monitoring survey of the majority of dwarf galaxies in the LG, with the Isaac Newton Telescope (INT) for a duration of three years [12]. Our main objective is to identify all Long Period Variable stars (LPVs) in them. Then, we can determine the star formation histories from the mass function of LPVs, with a method that we successfully applied in some of the LG galaxies [13, 14, 15, 16, 17]. The most evolved stars with low to intermediate birth mass,  $0.8 - 8 M_{\odot}$ , at the tip of the Asymptotic Giant Branch (AGB), and somewhat more massive red supergiants (RSGs), show brightness variations on timescales of  $\approx 100$  to  $> 1000$  days due to radial pulsations and this makes them powerful tools to trace stellar populations as young as  $\sim 30$  Myr to as old as the oldest Globular Clusters.

In this paper, we present a first census of LPV stars in Andromeda I (And I) dwarf galaxy with data from our survey. And I is a bright dSph ( $M_V = -11.8 \pm 0.1$  mag [18]), that was initially discovered on photographic plates by van den Bergh (1972). It lies some  $3.3^\circ$  from the center of M 31 at a position angle of  $\sim 135^\circ$  relative to the M 31 major axis [19]. Considerable efforts have been made to study the structure and properties of And I. For instance, McConnachie & Irwin (2006) have shown that And I is a strongly disrupted satellite of M 31. Also, they have derived some of the structural parameters such as position angle ( $22 \pm 15$  deg), ellipticity ( $0.22 \pm 0.04$ ), tidal radius ( $10.4 \pm 0.9$  arcmin) and half-light radius ( $2.8$  arcmin) for this galaxy [18]. Kalirai et al. (2010) with spectroscopic data of And I have calculated the mean radial velocity  $375.8 \pm 1.4$  km/s and intrinsic dispersion velocity  $10.6 \pm 1.1$  km/s. They determined a metallicity of  $-1.45 \pm 0.04$  using theoretical isochrones [20]. Recent studies have shown that a large fraction of the M 31 dwarf galaxies such as And I have extended star formation histories, and appear inconsistent with an early truncation of their star formation histories [21].

The distance to And I has been determined *via* several methods. Da Costa et al. (1996) determined a distance of  $810 \pm 30$  kpc by using Horizontal Branch stars, i.e. a distance modulus  $24.55 \pm 0.08$  mag [19]. By using the tip of the red giant branch (RGB), McConnachie et al. (2004) found a distance of  $735 \pm 23$  kpc, i.e. a distance modulus  $24.33 \pm 0.07$  mag [22]. However, Conn et al. (2012) revised this to  $\mu = 24.31 \pm 0.05$  mag. Martínez-Vázquez et al. (2017) calculated the distance based on the properties of the RR Lyrae stars and several independent techniques [23]: the reddening-free period-Wesenheit relations ( $24.49 \pm 0.08$ ), the luminosity-metallicity ( $M_V$  versus  $[\text{Fe}/\text{H}]$ ) relation ( $24.54 \pm 0.16$ ), the first overtone blue edge relation ( $24.49 \pm 0.10$ ) and the RGB tip method ( $24.49 \pm 0.12$ ) [24]. In this paper, we adopted the last one, i.e. a distance modulus  $24.49 \pm 0.12$  mag.

This paper is organized as follows: In Section 2, we describe the observations performed for this data set. Section 3 explains the data reduction and photometry method. The quality of data is discussed in section 4 and our method to detect LPVs is presented in Section 5. The discussion follows in Section 6.

## 2 Description of observations

Over the period June 2015 – October 2017, we used the Wide Field Camera (WFC) to conduct a survey of the majority of dwarf galaxies in the LG. The WFC is an optical mosaic camera at the 2.5m Isaac Newton Telescope (INT) of the Observatorio del Roque de los Muchachos (La Palma). It consists of four  $2048 \times 4096$  CCDs, with a pixel size of  $0.33$  arcsec/pixel. The edge to edge limit of the mosaic, neglecting the  $\sim 1'$  inter-chip spacing, is  $34.2'$ .

LPVs vary on timescales from  $\sim 100$  days for low-mass AGB stars to  $\sim 1300$  days for the dustiest massive AGB stars. Although we are not aiming to determine accurate periods,

Table 1: Log of WFC observations of And I dwarf galaxy.

Date (y m d)	Julian date	Epoch	Filter	$t_{\text{exp}}$ (sec)	Airmass
2016 02 09	2457428.3494	2	<i>i</i>	60	1.475
2016 06 14	2457553.6758	3	<i>i</i>	60	1.612
2016 08 10	2457610.6268	4	<i>i</i>	60	1.086
2016 08 12	2457612.6985	4	<i>V</i>	80	1.014
2016 10 20	2457681.6113	5	<i>i</i>	60	1.189
2016 10 20	2457681.6286	5	<i>V</i>	80	1.263
2017 01 29	2457783.4433	6	<i>i</i>	60	2.393
2017 08 01	2457966.7014	7	<i>i</i>	60	1.018
2017 08 01	2457966.7174	7	<i>V</i>	80	1.014
2017 09 01	2457997.5625	8	<i>i</i>	60	1.087
2017 09 01	2457997.5799	8	<i>V</i>	80	1.054
2017 10 06	2458033.4097	9	<i>i</i>	60	1.286
2017 10 08	2458034.5389	9	<i>V</i>	80	1.014

to identify the LPVs and to determine their amplitude and mean brightness, we required monitoring over several epochs, spaced by a month or more. The first epoch was June 2015, and the last was completed in October 2017. Unfortunately, we could not obtain data in October 2015 due to bad weather conditions and we observed a total of 9 epochs.

Observations were taken in the WFC Sloan *i* and Harris *V* filters. We selected *i* band because the spectral energy distribution (SED) of cool evolved stars peaks around  $1 \mu\text{m}$ , thus enhancing the contrast between the LPVs and other, warmer stars. Also, the bolometric correction needed to determine the luminosity in this band is smallest and least dependent on the colour and hence most accurate, and the effects of attenuation by dust are minimal. For monitoring the variations in temperature – and thus radius<sup>1</sup> – and to have more accurate SED modeling, we also observed in *V* band on several occasions to obtain colour information.

We chose exposure times that yield sufficient signal-to-noise ( $S/N$ ) to detect small changes in magnitude at different epochs. *i* band amplitudes of pulsating AGB stars are  $> 0.1$  mag. Therefore, we aimed for  $S/N = 10$  for the faintest stars, equivalent to the tip of the RGB. In order to cover the chip gaps of WFC and increase the  $S/N$ , the galaxy is observed 9 times with offsets of  $30''$  between the pointings each night. Additional observations were made of fields with photometric standard stars to be used for photometric calibration. The details of the observations used in this survey only for And I dwarf galaxy are listed in Table 1.

### 3 Data processing

The raw images can not be used for scientific analysis before they are combined, calibrated and corrected for artefacts. For this data reduction process, we used THELI (Transforming HEavenly Light into Image), an image processing pipeline for optical images taken by multi-chip (mosaic) CCD cameras [25]. It consists of a number of shell scripts that each perform a specific task and can be run in parallel on multi-chip CCDs. At first, image files are separated into frames of the individual chips (4 CCD chips in a WFC mosaic) and from then on, work is done on individual chips rather than whole images. Next, instrumental signatures

<sup>1</sup>Radius  $R$  and temperature  $T_{\text{eff}}$  are related via the luminosity  $L$  by the well-known formula  $L = 4\pi R^2 \sigma T_{\text{eff}}^4$

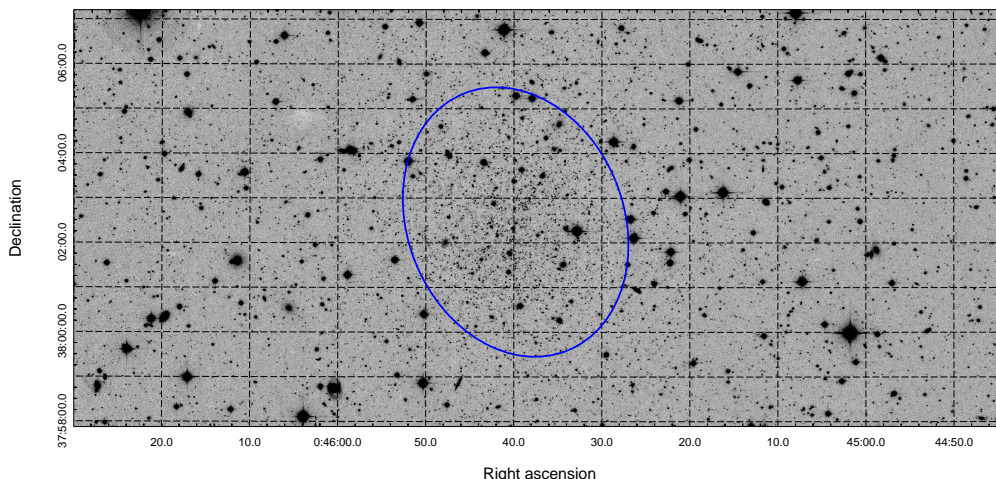


Figure 1: The master WFC image of And I dwarf galaxy. The half-light radii is marked with blue ellipse.

are removed from the data: the electronic offset (bias), pixel response and instrumental throughput variations (flatfield) and interference in the back-illuminated thinned detector chip, especially prevalent at the reddest wavelengths which more closely match the physical thickness of the chip (fringe pattern). While this process is repeated for all of the optical data, the subsequent step strongly depends on the scientific objectives and on the kind of data at hand. The data can be combined, optimised for astrometric accuracy, or optimised for automatised aperture photometry. Because of the crowded nature of the data in the direction of And I itself, it is more important at this stage to obtain accurate astrometry because the photometry will be done based on fitting and subtracting the individual stellar images.

Fortunately, in the THELI pipeline more emphasis is put on precise astrometry than precise photometry and it is perfectly suited to our goal. THELI uses the LDAC (Leiden Data Analysis Center) catalogue format, astronomical object catalogues created by Erik Deul and Emmanuel Bertin [26], and SCAMP package, astrometric tool developed in particular for multi-chip cameras [27], to create a full astrometric solution taking into account the gaps between the chips and overlapping objects. A useful feature of THELI is that it creates weights for individual frames. The weights are created based on the normalized flats. They mask defects such as cosmics and hot pixels in the images. The responsibility of the pipeline ends with the co-addition step. Sky background calculated with the SEXTRACTOR (software for source extraction) package [28] is subtracted from all frames and finally, the SWARP package [29] in THELI creates a co-added image using a weighted mean method [30].

To perform photometry in our crowded stellar field, we used the DAOPHOT/ALLSTAR software developed by Peter Stetson (1987). This package employs a Point Spread Function (PSF) method [31]. After identifying stars (from peaks above the noise) and obtaining aperture photometry for them, about 50–70 isolated stars were chosen in each frame to build an initial PSF model. By subtracting all but the PSF model stars from the frame, a final PSF model was build. Then ALLSTAR subtracts all the stars of image with using PSF fitting photometry along with the current best guesses of their positions and magnitudes.

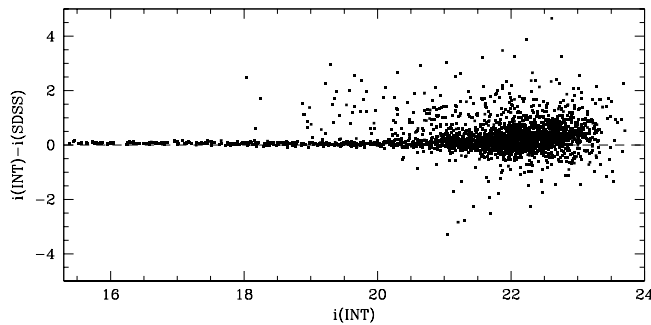


Figure 2: Magnitude differences between INT catalogue and SDSS of And I dwarf galaxy, plotted against  $i$  magnitude of our catalogue.

The individual images were aligned using the DAOMASTER routine, which computes the astrometric transformation equation coefficients from the ALLSTAR results. We combined the individual images using the MONTAGE2 routine [32] to create a master mosaic of And I (Fig. 1) and then a master catalogue of stars. This master catalogue was used as input for ALLFRAME, which simultaneously performed PSF-fitting photometry on these stars within each of the individual images. In this way, our final catalogue for And I was made.

To determine aperture corrections to the PSF-fitting photometry, i.e. the difference between the PSF-fitting and large-aperture magnitude of these stars, we used the DAOGROW routine [33]. It constructs growth-curves for each frame from which all stars had been subtracted except the PSF stars. We then applied the COLLECT routine [34] to calculate the aperture correction. We added this value to each of the PSF-fitting magnitudes using the NEWTRIAL routine [35].

Photometric calibration was then performed using the NEWTRIAL routine. Zero points were obtained for each frame based on the standard field observations. To obtain accurate zero points in the Sloan  $i$  filter, we applied transformation equations derived from comparing Stetson’s compilation of the Landolt standard stars with the corresponding SDSS DR4 photometry [36]. For frames obtained on nights without standard star measurements, we adopted the average of zero points from other nights. Airmass-dependent atmospheric extinction corrections were applied adopting the extinction coefficients determined for La Palma [37].

In order to estimate the accuracy of calibration, we cross correlated the results with the SDSS. The matches were obtained by performing search iterations using growing search radii, in steps of  $0.1''$  out to  $1''$ , on a first-encountered first-associated basis but after ordering the principal photometry in order of diminishing brightness (to avoid rare bright stars being erroneously associated with any of the much larger numbers of faint stars). As shown in Fig. 2, the result is consistent with good accuracy with SDSS catalogue within our desired range ( $21 > i > 18$  mag, see below).

## 4 Quality assessment

To estimate the completeness of our catalogue, we used the ADDSTAR routine in the DAOPHOT package [31]. This task can add synthetic stars to an image, either placed at random by the computer or in accordance with positions and magnitudes specified by us. All photometric are then applied to the new images and so the star-finding efficiency and the photometric

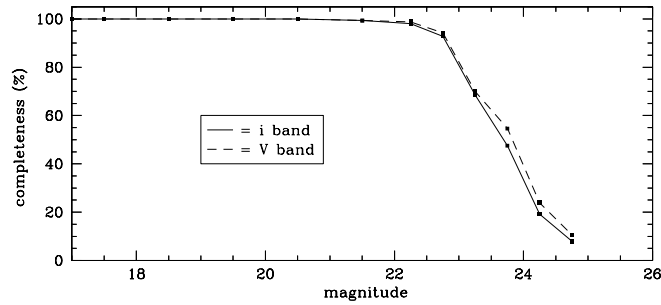


Figure 3: Completeness as a function of *i*-band (solid line) and *V*-band (dashed line) magnitude.

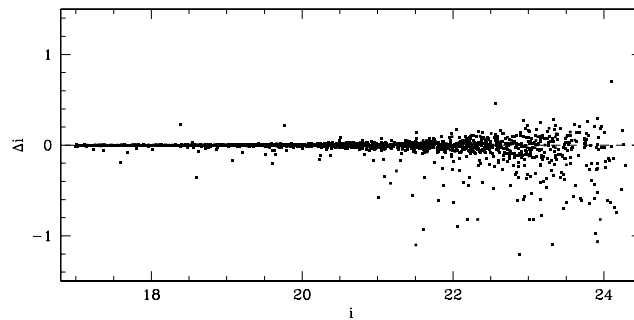


Figure 4: The difference between the input stellar magnitudes and the recovered stellar magnitudes from the artificial star tests.

accuracy can be estimated by comparing the output data for these stars to what was put in.

To avoid small number statistics in the artificial-star analysis without significantly changing the properties of the field (crowdedness), we added 300 artificial stars in each of 8 trials to the master mosaic and two of the individual frames in different bands in 1-mag bins starting from  $i = 17$  mag until  $i = 25$  mag (for *V* the same as *i*). Stars were positioned randomly in the image and Poisson noise was added. Then, we repeated the DAOPHOT/ALLSTAR/ALLFRAME procedure on the new frames as described before. Once the photometry was done and the final list created, we used DAOMASTER to evaluate what fraction of stars was recovered. As one can see in Fig. 3, our catalogue is essentially complete down to  $i \sim 22$  mag (near the RGB-tip, see below), dropping to below 50% at  $i = 23.6$  mag. The *V*-band reaches similar completeness levels but at  $\sim 0.1$  magnitude fainter.

The result of estimating the accuracy of our photometry is shown in Fig. 4. The difference between the input stellar magnitudes and the recovered magnitudes down to  $i \sim 22$  mag is very small,  $|\Delta i| < 0.1$  mag, but it increases for fainter magnitudes. So, this photometry is deep enough to meet the scientific objectives of our project of studying AGB stars and RSGs, because they have  $i < 21.5$  mag – except possibly for heavily dust-enshrouded cases, which however are rare.

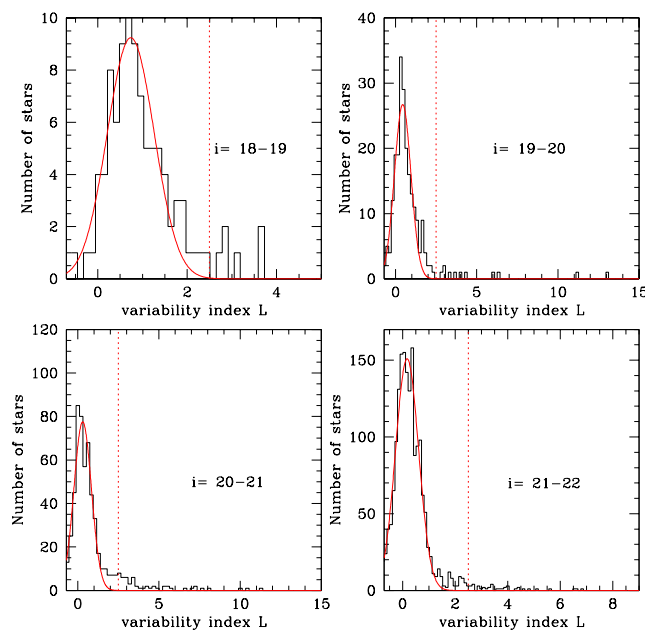


Figure 5: Histograms of the variability index  $L$ , for several  $i$ -band magnitude bins. The solid lines show Gaussian functions fitted to the histograms.

## 5 Variability analysis

For finding variable star candidates, we used the NEWTRIAL program [34]. This program was introduced by Welsh & Stetson (1993) and developed further by Stetson (1996). In this method, the observations are paired on the basis of timespan between observations such that the observations of each pair have a timespan less than the shortest period expected for the kind of the variable stars of interest (100 days or longer for LPVs). If within a pair of observations only one measurement is available for a particular star then the weight of the pair for that star is set to 0.5.

The NEWTRIAL program first calculates the  $J$  index:

$$J = \frac{\sum_{k=1}^N w_k \text{sign}(P_k) \sqrt{|P_k|}}{\sum_{k=1}^N w_k}. \quad (1)$$

Here, observations  $i$  and  $j$  have been paired and each pair  $k$  has been given a weight  $w_k$ ; the product of the normalized residuals,  $P_k = (\delta_i \delta_j)_k$ , where  $\delta_i = (m_i - \langle m \rangle) / \epsilon_i$  is the deviation of measurement  $i$  from the mean, normalized by the error on the measurement,  $\epsilon_i$ . Note that  $\delta_i$  and  $\delta_j$  may refer to measurements taken in different filters ( $P_k = \delta^2 - 1$  if  $i = j$ ). The  $J$  index has a large positive value for variable stars and tends to zero for data containing random noise only.

When we are dealing with a small number of observations or corrupt data we gain from also calculating the Kurtosis index:

$$K = \frac{\frac{1}{N} \sum_{i=1}^N |\delta_i|}{\sqrt{\frac{1}{N} \sum_{i=1}^N \delta_i^2}}. \quad (2)$$

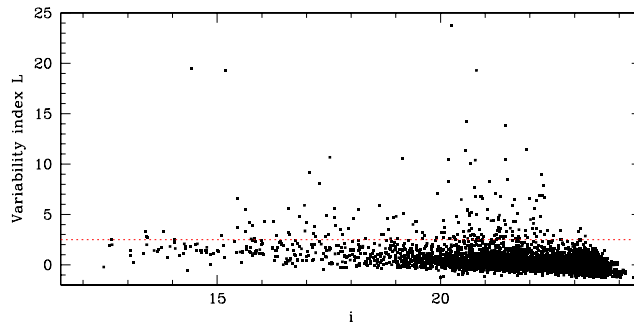


Figure 6: Variability index  $L$  vs.  $i$ -band magnitude. The dashed line indicates our threshold for identifying variable stars, at  $L > 2.5$ .

The value of  $K$  depends on the shape of the light-curve:  $K = 0.9$  for a sinusoidal light variation, where the source spends most time near the extrema,  $K = 0.798$  for a Gaussian distribution, which is concentrated towards the average brightness level (as would random noise), and  $K \rightarrow 0$  for data affected by a single outlier (when  $N \rightarrow \infty$ ).

Also, there is a variability index that depends on both the  $J$  and  $K$  indices [35]:

$$L = \frac{J \times K \sum_{i=1}^N w_i}{0.798 w_{\text{all}}}, \quad (3)$$

where  $\sum w$  is the total weight assigned to a given star and  $w_{\text{all}}$  is the total weight a star would have if observed in every single observation. We used  $L$  variability index for finding variable stars in this paper. One reason for using it is that the lightcurves of LPVs have shapes roughly between sinusoidal and triangular, and thus a kurtosis near 0.9-1. The  $L$  index is weighted by that kurtosis, making it larger for such variations compared to more random or erratic variations.

To determine the optimal variability threshold, we plotted histograms of the variability index for several  $i$ -band magnitude intervals in the range 18–22 mag along with a fitted Gaussian function to each of them. As shown in Fig. 5, while the Gaussian function is a near-perfect fit to the symmetrical distributions at low values for  $L$ , the distributions show a pronounced tail towards higher values for  $L$ . The departure from the Gaussian shape occurs typically around  $L \approx 2.5$ . Fig. 6 shows how the variability index  $L$  varies with  $i$ -band magnitude. The dashed line indicates our threshold for detected variability:  $L > 2.5$ .

The number of variable stars are suspect and we inspected all of the stars by eye. Some of these stars are located near the edge of the frame and some others located on the site of a saturated star in image, resulting in particularly poor photometry on several epochs with distorted stellar profiles and therefore, they are unreliable. We removed these stars and thus identified 116 variable stars in the And I. Two examples of likely long-period variability are shown in Fig. 7, with a non-variable star for comparison. One of the variable stars was also found to be variable at mid-IR wavelengths in the *Spitzer* monitoring survey DUSTiNGS [38] (cf. Section 6).

## 5.1 Amplitudes of variability

A measure for the amplitude of variability can be obtained by assuming a sinusoidal light-curve shape. It is done by comparing the standard deviation in the magnitudes to that

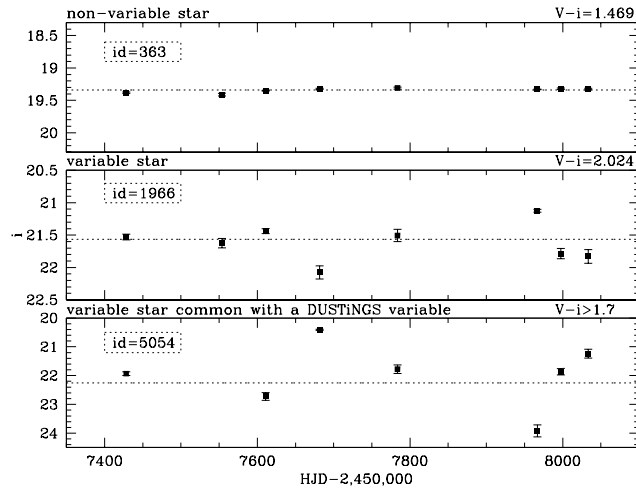


Figure 7: Example light-curves of two variable stars, with #5054 in common with the DUSTiNGS catalogue of variable *Spitzer* sources [38], with a non-variable star in the top panel for comparison.

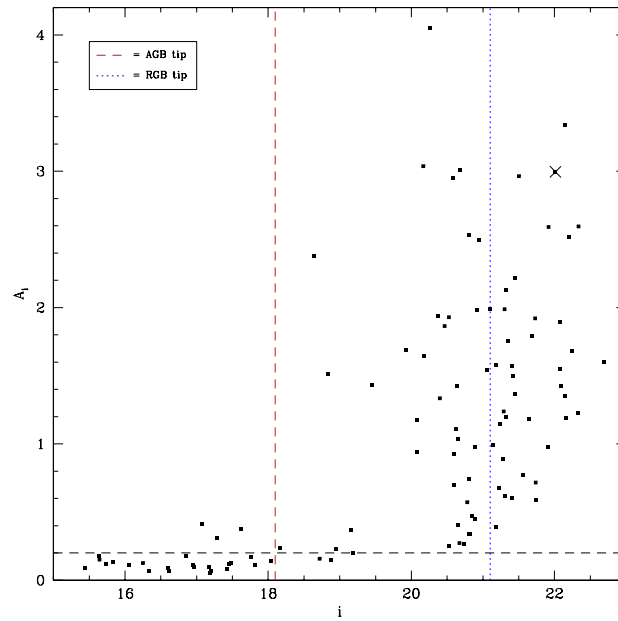


Figure 8: Estimated amplitude,  $A_i$ , of variability *vs.*  $i$ -band magnitude.

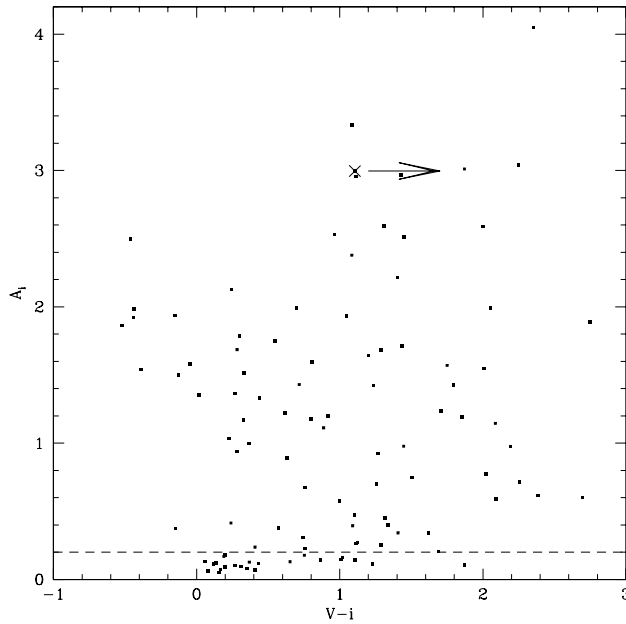


Figure 9: Estimated amplitude,  $A_i$ , of variability *vs.* colour.

expected for a completely random sampling of a sinusoidal variation. The estimated  $i$ -band amplitude of variability is plotted *vs.*  $i$ -band magnitude in Fig. 8. Variability could have been detected for  $A_i > 0.2$  mag. There is a clear tendency for the amplitude to diminish with increasing brightness, which is a known [39, 40, 41] and to some extent understood [42] trend for AGB stars. The amplitudes stay below  $A_i \sim 4.2$  mag and generally  $A_i < 2.5$  mag. Very dusty AGB stars are known to reach such large amplitudes [39, 40, 41], but they are very rare. One example of such star, #5054 is highlighted in Fig. 8 with a cross; its lightcurve is displayed in Fig. 7 and it was also identified as a mid-IR variable by the DUSTiNGS survey [38]. The most interesting stars might be those three brighter than the tip of the AGB and with amplitude about 0.3–0.4 mag. They could be very massive AGB stars undergoing Hot Bottom Burning or RSGs and therefore, represent a “young” population ( $< 100$  Myr).

The estimated  $i$ -band amplitude of variability is plotted *vs.* the  $V - i$  colour in Fig. 9. Stars towards redder colours have larger amplitudes. This is not surprising as large-amplitude variability is known to be associated with abundant dust formation [39, 40, 41]. For the DUSTiNGS variable (#5054), we estimated  $V > 23.7$  and thus  $(V - i) > 1.7$  due to the completeness limit in  $V$ -band (23.7 mag).

## 6 Discussion

Our final catalogue contains 10585 stars in the region of CCD 4 of WFC ( $11.26 \times 22.55$  arcmin<sup>2</sup>), with And I located near its center. Fig. 10 presents the spatial location of our variable candidates. The half-light radii is marked with a blue ellipse. The density of variable stars for the regions inside and outside the ellipse are 0.68 and 0.43 number/arcmin<sup>2</sup>, respectively.

Colour–magnitude diagrams of this galaxy in  $i$ -band and  $V$ -band *vs.*  $(V - i)$  colour are

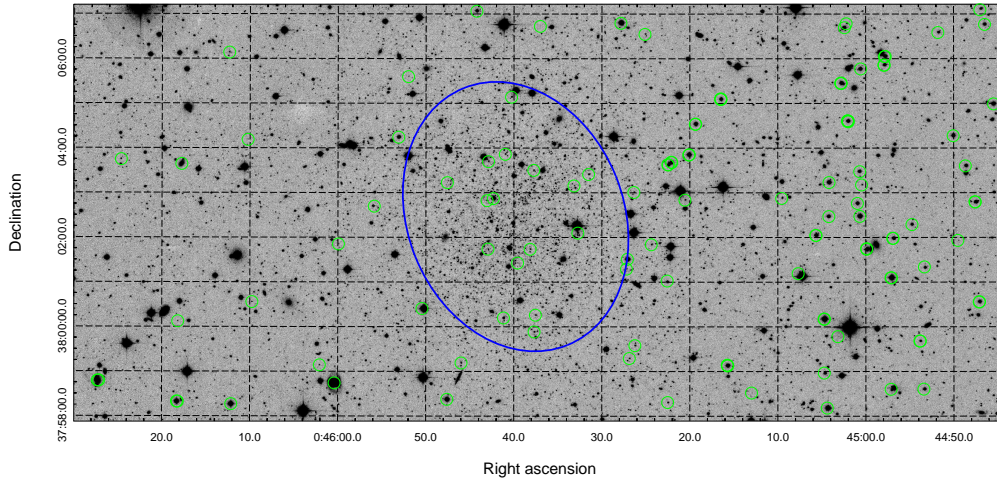


Figure 10: The master WFC image of And I dwarf galaxy with spatial location of our variable candidates. The half-light radii is marked with blue ellipse.

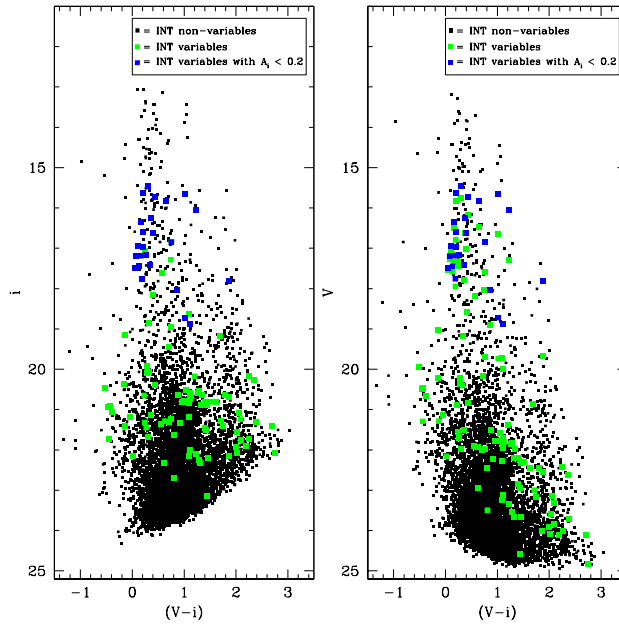


Figure 11: colour-magnitude diagrams showing the variable stars in green. The variable stars with  $A_i < 0.2$  mag are highlighted in blue.

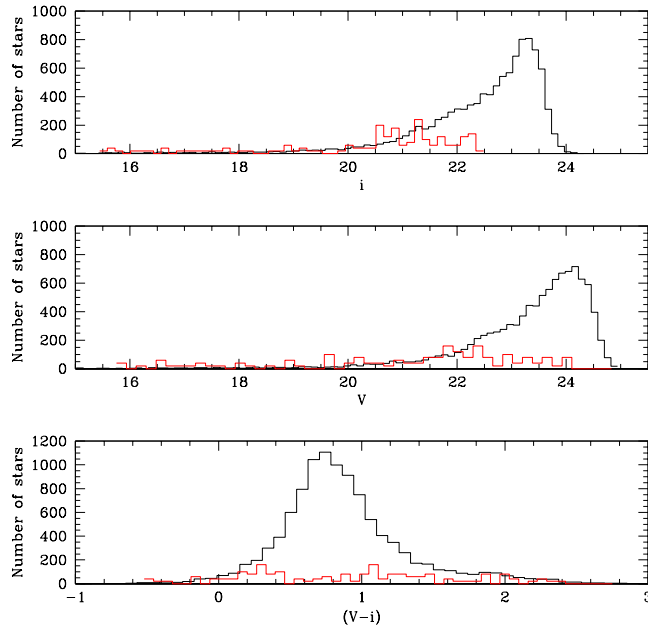


Figure 12: Distribution of all INT sources (black) and INT variable stars (red) as a function of brightness and colour. we multiplied the variable stars' histograms by 20.

shown in Fig. 11. The variable stars we identified are highlighted in green. These are mainly found between  $i \sim 18$ – $22$  mag, and as the stars get fainter, their number decreases. Some brighter variable RSGs are found (around  $i \sim 16$ – $18$  mag), too.

Fig. 12 presents histograms of the distributions over brightness and colour. The largest fraction of stars that are found to be variable occurs between  $i \sim 18$ – $22$  mag. As the frequency of stars increases from  $i \sim 22$  mag, the frequency of variable stars decreases. This is probably because many stars have not yet reached the final phase of their evolution and they will still evolve to higher luminosities and lower temperatures before they develop large-amplitude variability.

To assess the level of contamination by foreground stars, we performed a simulation with the TRILEGAL tool [43]. We simulated two different sizes of the field, a  $0.07 \text{ deg}^2$  (about the size of the entire CCD4 of WFC) and a  $0.007 \text{ deg}^2$  (half the light of the galaxy), in the direction ( $l = 121.68^\circ$ ,  $b = -24.82^\circ$ ). As shown in Fig. 13 the foreground stars have contaminated our desired areas; therefore, the distribution of the population of AGB stars and then the star formation history can not be obtained from colour–magnitude diagrams alone. Because LPVs are relatively rare, and become rare still in directions away from the Galactic plane, one could instead use the distributions over LPVs to chart the star formation history, relatively free from foreground contamination.

The stellar population in the And I dwarf galaxy can be described using isochrones calculated by Marigo et al. (2008) (Fig. 14) [44]. The isochrones were calculated for And I metallicity,  $Z = 0.00069$  [20]. The 100-Myr and 1-Gyr isochrones show consistency with the red branch of INT variables. The 10-Gyr isochrone defines the location of tip of the RGB, that here is 21.1 mag for  $i$  band. These isochrones are the most appropriate theoretical models for our purpose, for the following reasons:

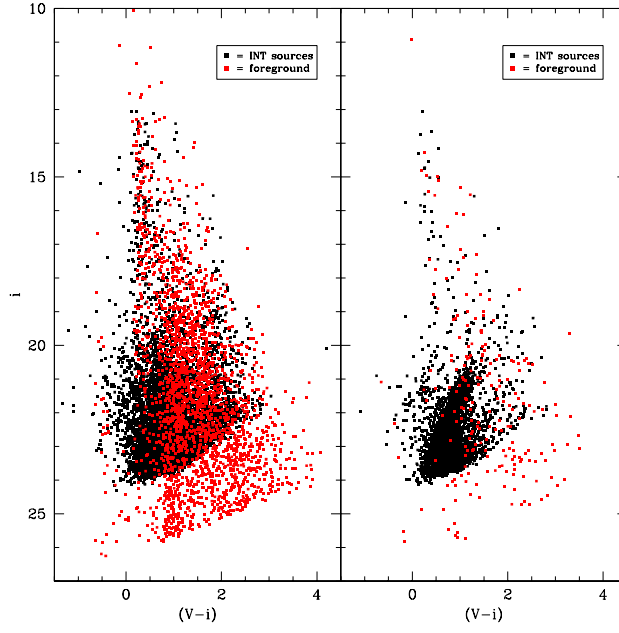


Figure 13: Estimated contamination by foreground stars (in red), from a simulation with TRILEGAL [43]. In the left panel, a  $0.07 \text{ deg}^2$  field is considered while in the right panel, we have a  $0.007 \text{ deg}^2$  field centered on And I (half the light of the galaxy).

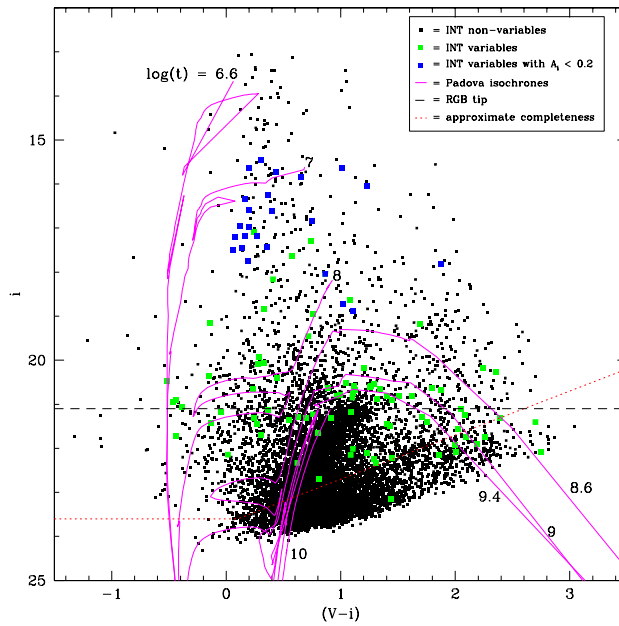


Figure 14: colour-magnitude diagram of  $(V - i)$ , with variable stars highlighted in green. The variable stars with  $A_i < 0.2$  mag are highlighted in blue. Overplotted are isochrones from Marigo et al. (2008) for And I with a distance modulus of  $24.49 \text{ mag}$  [23].

- The star’s evolution is followed all the way through the thermal pulsing AGB until the post-AGB phase. Crucially, two important phases of stellar evolution are included, viz. the third dredge-up mixing of the stellar mantle as a result of the helium-shell burning phase, and the enhanced luminosity of massive AGB stars undergoing hot bottom burning (HBB) [45];
- The molecular opacities which are important for the cool atmospheres of evolved stars have been considered in the models of stellar structure. The transformation from oxygen-dominated (M-type) AGB stars to carbon stars in the birth mass range  $M \sim 1.5\text{--}4 M_{\odot}$  is accounted for [46];
- The dust production in the winds of LPVs, and the associated reddening is included;
- The radial pulsation mode is predicted;
- Combination of their own models for intermediate-mass stars ( $M < 7 M_{\odot}$ ), with Padova models for more massive stars ( $M > 7 M_{\odot}$ ) [47]), gives a complete coverage in birth mass ( $0.8 < M < 30 M_{\odot}$ );
- Magnitudes are calculated on a wide range of common optical and IR photometric systems;
- The isochrones are available via an internet-based form in a user-friendly format.

## 6.1 Cross-identifications in other catalogues

We cross-correlate our INT variability search results with the mid-IR variability search performed with the *Spitzer* Space Telescope [11] and also, with the variables catalogue obtained with the *Hubble* Space Telescope (HST) data [23]. The matches were obtained by search iterations using growing search radii, in steps of  $0.1''$  out to  $1''$ , on a first-encountered first-associated basis after ordering the principal photometry in order of diminishing brightness (*i*-band/I-band for the optical catalogues, and  $3.6\text{-}\mu\text{m}$  band for the *Spitzer* catalogue).

DUSTiNGS (DUST in Nearby Galaxies with *Spitzer*) was a  $3.6$  and  $4.5 \mu\text{m}$  post-cryogen *Spitzer* Space Telescope imaging survey of 50 dwarf galaxies within 1.5 Mpc that was designed to identify dust-producing AGB stars and massive stars [11]. Using 2 epochs, spaced approximately 6 months apart, they identified a total of 4 variable stars for And I. As a result of cross-correlating, we obtained 5616 common stellar sources between our photometric catalogue and the DUSTiNGS survey in a  $0.07$  square degree field centered on And I. As shown in Fig. 15, all four of their variable stars are listed in our identified variables catalogue. We found a few variables among the brighter red giants, including a red one, at  $[3.6] - [4.5] = 1$  mag. We did not find variables above the tip of the 10 million year isochrone, which is consistent with there being no LPVs among stars more massive than those which become RSGs. Also we did not find variables among the redder sources,  $[3.6] - [4.5] > 0.4$  mag, around  $[3.6] \sim 17 - 18$  mag. Is it possible that these sources have only been detected in our survey in one epoch, when they were near maximum brightness, so we could not determine any variability.

Martínez-Vázquez et al. (2017) presented the ISLAndS (Initial Star formation and Lifetimes of Andromeda Satellites) project, providing a census of variable stars in six M31 dSph satellites observed with the HST. They detected 296 RR Lyrae stars in And I [23]. There are 59 objects in common between their survey and ours, among which only two were identified by us as variable (Fig. 16). This illustrates that these surveys probe entirely different, complementary populations – the oldest populations (ISLAndS) and the intermediate-age and younger populations (our survey).

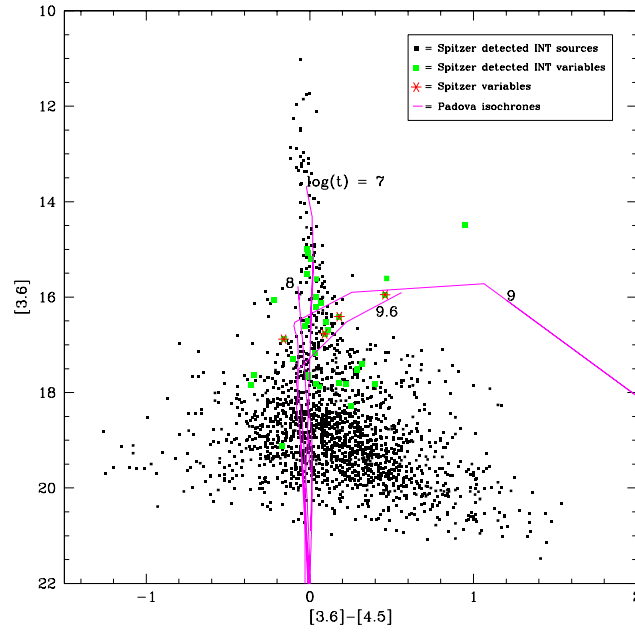


Figure 15: Mid-IR colour–magnitude diagram from DUSTiNGS survey, with INT variables highlighted in green and the variable stars of DUSTiNGS in red asterisks. Isochrones from Marigo et al. (2008) for 10 Myr, 100 Myr, 1 Gyr and 4 Gyr are drawn.

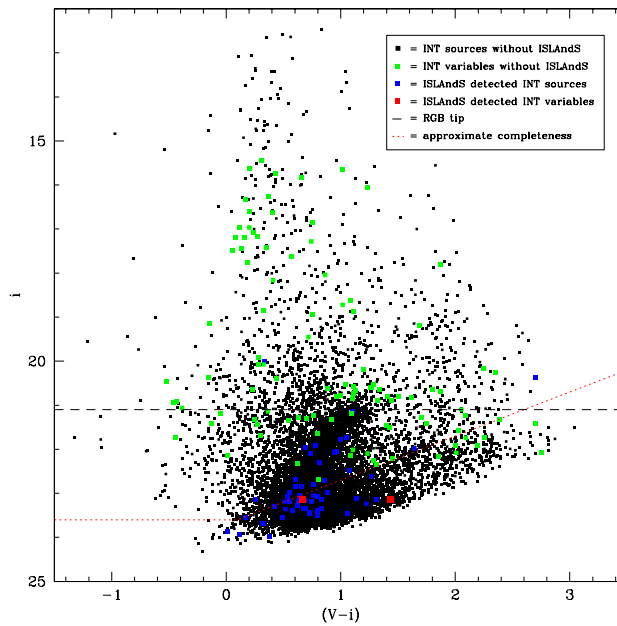


Figure 16: Optical colour–magnitude diagram showing the stars from the INT survey that were and were not detected in the ISLANDS variability survey [23]. Two red points represent common variable stars between the two surveys.

## 7 Conclusions

We have presented the preliminary, initial results from our long-term optical monitoring campaign at the Isaac Newton Telescope of a sample of the LG dwarf galaxies, namely for the And I satellite of M31. We found 116 variable stars, including a few among the brighter and redder sources, some of which have also been detected at mid-IR wavelengths. This indicates the presence of stars around a Gyr or younger in And I, which contribute to the replenishment of the interstellar medium within And I.

## Acknowledgments

The observing time for this survey is provided by the Iranian National Observatory and the UK-PATT allocation of time to programmes I/2016B/09 and I/2017B/04 (PI: J. van Loon). The observers thank the Iranian National Observatory and the School of Astronomy (IPM) for the financial support of this project. The first author also thanks the School of Astronomy for the research grant. We thank the ING observers for service mode observations. Also, we thank Alireza Molaeinezhad, Arash Danesh, James Bamber and Iain McDonald for their efforts during the observations. We are grateful to Peter Stetson for sharing his photometry routines, Marta Boyer and Clara Martínez-Vázquez for sending us their full variability catalogue.

## References

- [1] Mateo M., Olszewski E. W., Vogt S. S., Keane M. J., 1998, *AJ*, 116, 2315
- [2] Kleyna J. T., Wilkinson M. I., Evans N. W., Gilmore G., 2004, *MNRAS*, 354, L66
- [3] Gilmore G., et al., 2007, *ApJ*, 663, 948
- [4] Walker M. G., Mateo M., Olszewski E. W., Peñarrubia J., Evans N.W., Gilmore G. 2009, *ApJ*, 704, 1274
- [5] Wolf J., et al., 2010, *MNRAS*, 406, 1220
- [6] Dolphin A. E., Weisz D. R., Skillman E. D., Holtzman J. A., 2005, *ASP Conference Series*
- [7] Read J. I., Pontzen A. P., Viel M., 2006, *MNRAS*, 371, 885
- [8] Tolstoy E., Hill V., Tosi M., 2009, *ARA&A*, 47, 371
- [9] Weisz D. R., et al., 2011, *ApJ*, 743, 8
- [10] Kazantzidis S., Lokas E. L., Mayer L., Knebe A., Klimentowski J., 2011, *ApJL*, 740, L24
- [11] Boyer M. L., et al., 2015, *ApJ*, 216, 10
- [12] Saremi E., et al., 2017, *J. Phys.: Conf. Ser.*, 869, 012068
- [13] Javadi A., van Loon J. Th., Mirtorabi M. T., 2011a, *MNRAS*, 411, 263
- [14] Rezaeikh S., Javadi A., Khosroshahi H., van Loon J. Th., 2014, *MNRAS*, 445, 2214

- [15] Javadi A., et al., 2015, MNRAS, 447, 3973
- [16] Javadi A., van Loon J. Th., Khosroshahi H., Tabatabaei F., Golshan R. H., 2017, MNRAS, 464, 2103
- [17] Golshan R. H., Javadi A., van Loon J. Th., Khosroshahi H., Saremi E., 2017, MNRAS, 466, 1764
- [18] McConnachie A. W., Irwin M. J., 2006, MNRAS, 365, 1263
- [19] Da Costa G. S., Armandroff T. E., Caldwell N., Seitzer P., 1996, AJ, 112, 2576
- [20] Kalirai J. S., et al., 2010, ApJ, 711, 671
- [21] Martin N. F., et al., in press (arXiv:1704.01586)
- [22] McConnachie A. W., et al., 2004, MNRAS, 350, 243
- [23] Martínez-Vázquez., et al., in press (arXiv:1710.09038)
- [24] Conn A. R., et al., 2012, ApJ, 758, 1
- [25] Erben T., et al., 2005, AN, 326, 432
- [26] E.Deul, <ftp://ftp.strw.leidenuniv.nl/pub/ldac/software/>
- [27] Bertin E., 2006, ADASS XV: ASP Conf. Ser, 351, 112
- [28] Bertin E., Arnouts S., 1996, A&A Supplement, 117, 393
- [29] Bertin E., 2010, Astrophysics Source Code Library, 10068
- [30] Schirmer M., 2013, ApJ Supplement, 209, 2
- [31] Stetson P. B., 1987, PASP, 99, 191
- [32] Stetson P. B., 1994, PASP, 106, 250
- [33] Stetson P. B., 1990, PASP, 102, 932
- [34] Stetson P. B., 1993, in: Stellar Photometry Current Techniques and Future Developments, IAU Coll. Ser. 136, 291
- [35] Stetson P. B., 1996, PASP, 108, 851
- [36] Jordi K., Grebel E. K., Ammon K., 2006, A&A, 460, 339
- [37] García-Gil A., Muñoz-Tuñón C., Varela A. M., 2010, PASP, 122, 1109
- [38] Boyer M. L., et al., 2015 ApJ, 800, 51
- [39] Wood P. R., Whiteoak J. B., Hughes S. M. G., Bessell M. S., Gardner F. F., Hyland A. R., 1992, ApJ, 397, 552
- [40] Wood P. R., 1998, A&A, 338, 592
- [41] Whitelock P. A., Feast M. W., van Loon J. Th., Zijlstra A. A., 2003, MNRAS, 342, 86
- [42] van Loon J. Th., et al., 2008, A&A, 487, 1055

- [43] Girardi L., Groenewegen M. A. T., Hatziminaoglou E., da Costa L., 2005, *A&A*, 436, 895
- [44] Marigo P., Girardi L., Bressan A., Groenewegen M. A. T., Silva L., Granato G. L., 2008, *A&A*, 482, 883
- [45] Iben I. Jr., Renzini A., 1983, *ARA&A*, 21, 271
- [46] Marigo P., Girardi L., 2007, *A&A*, 469, 239
- [47] Bertelli G., Bressan A., Chiosi C., Fagotto F., Nasi E., 1994, *A&A*, 106, 275